Advances in Applied Mathematics and Mechanics
Adv. Appl. Math. Mech., Vol. **11**, No. 1, pp. 1-17

DOI: 10.4208/aamm.OA-2018-0175
October 2019

An Immersed Finite Element Method for Elliptic Interface Problems with Multi-Domain and Triple Junction Points

Yuan Chen[1], Songming Hou[2] and Xu Zhang[3,*]

[1] *Department of Environmental Science, Hohai University, Nanjing 210098, Jiangsu, China*
[2] *Department of Mathematics and Statistics, Louisiana Tech University, Ruston, LA 71272, USA*
[3] *Department of Mathematics and Statistics, Mississippi State University, Mississippi State, MS 39762, USA*

Received 1 August 2018; Accepted (in revised version) 29 March 2019

Abstract. Interface problems have wide applications in modern scientific research. Obtaining accurate numerical solutions of multi-domain problems involving triple junction conditions remains a significant challenge. In this paper, we develop an efficient finite element method based on non-body-fitting meshes for solving multi-domain elliptic interface problems. We follow the idea of immersed finite element by modifying local basis functions to accommodate interface conditions. We enrich the local finite element space by adding new basis functions for handling non-homogeneous flux jump. The numerical scheme is symmetric and positive definite. Numerical experiments are provided to demonstrate the features of our method.

AMS subject classifications: 35R05, 65N15, 65N30

Key words: Immersed finite element, interface problems, triple junction, multi-domain.

1 Introduction

The elliptic interface problems have raised much attention in the past decades and related numerical methods have been developed for solving interface problems accurately and efficiently. Conventional numerical methods, such as finite element method (FEM) [8], can be used to solve interface problems. These methods require the mesh to fit the interface; thus they are sometimes called fitted-mesh methods. A limitation of these methods

*Corresponding author.
Emails: chenyuan15@hhu.edu.cn (Y. Chen), shou@latech.edu (S. M. Hou), xuzhang@math.msstate.edu (X. Zhang)

is that the solution mesh has to be regenerated when dealing with a moving interface problem because of this body-fitting restriction.

Many numerical methods based on non-body-fitting meshes have been developed for solving interface problems. In the finite difference framework, since the pioneering work of Peskin [25] on the immersed boundary method, there have been the immersed interface method [20], the matched interface and boundary (MIB) method [30], the kernel-free boundary integral method [29], the embedded boundary method [16] and the cut-cell method [19]. In the finite element framework, there are generalized FEM [4], extended FEM [9], cut FEM [12] and the immersed finite element (IFE) method [21]. The IFE method was first introduced in [21] for one-dimensional interface problems with piecewise linear polynomial approximation. Since then, the method has been extended to multi-dimensional problems [10, 13, 22, 23], higher order approximations [2, 3, 6, 7] and interface problems of other partial differential equation models [1, 15, 24]. Moreover, the IFE method has also been extended to non-homogeneous flux jump conditions [11, 14].

So far, most IFE methods in the literature are designed to solve interface problems with two sub-domains. When it comes to multi-domain problems with intersecting interfaces, such as problems with triple interface junction points, the complexity of the problems will inevitably increase. There are a few numerical methods developed for multi-domain interface problems. In [17], the authors developed a Petrov-Galerkin type method for multi-domain problems with triple junction conditions and triple junction points, which is an extension from two-domain interface problems [18]. Another method is based on MIB framework [28] for scalar jumping coefficients. The bandwidth of the sparse linear system in [28] is usually larger than that in [17]. Some more recent work on multi-domain interface problems include the three dimensional problem in [26] and the elasticity problem in [27].

In this paper, we propose a numerical method based on IFE methods for solving the elliptic interface problem with triple-junction interfaces. We present the construction of IFE basis functions on interface elements with triple-junction points. Local and global IFE spaces will be formulated accordingly. Moreover, we extend the construction for handling the non-homogeneous flux jump following the idea in [14]. Compared with previous methods in [17], there are two improvements in the method in this paper. First, the construction of IFE basis function covers more types of geometrical configuration of interface elements. To be more specific, there is no need for the assumption in [17] that a triple junctional interface must intersect with three different edges of an element. The second advantage of this method is that the stiffness matrix of linear system is always symmetric positive definite, compared with the non-symmetric positive definite matrix in [17].

The rest of article is organized as follows. In Section 2, we introduce the elliptic interface problem with multi-domain and triple junction interfaces and derive its weak formulation. In Section 3, we construct the local IFE basis functions and the non-homogeneous flux basis functions on different types of interface elements. Then we formulate the local and global IFE spaces and apply them for solving the multi-interface problem. In Section

4, some numerical experiments are provided to demonstrate the accuracy of our method. Brief conclusion is drawn in Section 5.

2 Interface problems and weak formulation

In this section, we first describe the elliptic equation with multiple intersecting interfaces.

Let $\Omega \subset \mathbb{R}^2$ be an open bounded domain. We assume that Ω is divided by multiple interfaces into subdomains. Without loss of generality, we consider the case with three intersecting interfaces. We assume that the interfaces Γ_1, Γ_2 and Γ_3 divide Ω into disjoint open subdomains Ω_1, Ω_2 and Ω_3. We also assume that the boundaries $\partial\Omega$ and $\partial\Omega_i$, $i=1,2,3$ are Lipschitz continuous. The unit normal vectors of Γ_i, $i=1,2,3$ are denoted by $\mathbf{n}_i$. The intersecting points of Γ_i are called the triple junction point. See Fig. 1 for an illustration of the geometrical setting.

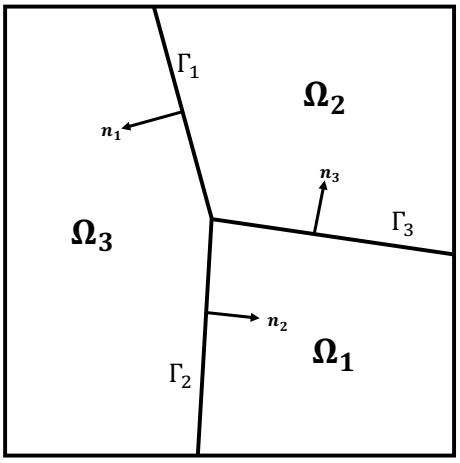

Figure 1: A typical triple-interface domain.

We consider the following elliptic interface problem defined on this triple junction domain:

$$-\nabla\cdot(\beta\nabla u) = f \qquad \text{in } \Omega_1\cup\Omega_2\cup\Omega_3, \tag{2.1a}$$

$$u = g \qquad \text{on } \partial\Omega. \tag{2.1b}$$

Here, the coefficient function β is discontinuous across the interfaces such that $\beta(\mathbf{x})=\beta_i$, for $\mathbf{x}\in\Omega_i$, $i=1,2,3$ where $\beta_i>0$ are positive constants. The source function f and the boundary function g are given. For simplicity, we denote $g_i = g|_{\partial\Omega\cap\partial\Omega_i}$ from now on. Across the interfaces Γ_i, the solution u is assumed to be continuous, i.e.,

$$[u]_{\Gamma_i}=0, \quad \forall i=1,2,3. \tag{2.2}$$

The normal flux jump are prescribed as follows:

$$\begin{cases} [\beta\nabla u\cdot\mathbf{n}]_{\Gamma_1}=(\beta_3\nabla u_3-\beta_2\nabla u_2)\cdot\mathbf{n}_1=b_1(x,y) & \text{on } \Gamma_1, \\ [\beta\nabla u\cdot\mathbf{n}]_{\Gamma_2}=(\beta_1\nabla u_1-\beta_3\nabla u_3)\cdot\mathbf{n}_2=b_2(x,y) & \text{on } \Gamma_2, \\ [\beta\nabla u\cdot\mathbf{n}]_{\Gamma_3}=(\beta_2\nabla u_2-\beta_1\nabla u_1)\cdot\mathbf{n}_3=b_3(x,y) & \text{on } \Gamma_3. \end{cases} \tag{2.3}$$

Here, $u_i=u|_{\Omega_i}$ and b_i, $i=1,2,3$ are given functions defined on Γ_i.

Multiplying the Eq. (2.1a) by a test function $v\in H_0^1(\Omega)$, taking integral on each subdomains Ω_i and using Green's formula and the jump conditions (2.2)-(2.3), we can obtain the variational form of the interface problem: Find $u\in H^1(\Omega)$ such that $u|_{\partial\Omega}=g$ and

$$\sum_{i=1}^{3}\int_{\Omega_i}\beta\nabla u\cdot\nabla v dxdy=\int_{\Omega}fvdxdy-\sum_{i=1}^{3}\int_{\Gamma_i}b_i v ds,\quad \forall v\in H_0^1(\Omega). \tag{2.4}$$

Define the broken Sobolev space

$$\tilde{H}^2(\Omega)=\left\{v\in H^1(\Omega):v|_{\Omega_i}\in H^2(\Omega_i),\ [\beta\nabla u\cdot\mathbf{n}]_{\Gamma_i}=b_i,\ i=1,2,3\right\},$$

equipped with the norm

$$\|u\|^2_{\tilde{H}^2(\Omega)}=\|u\|^2_{H^1(\Omega)}+\sum_{i=1}^{3}|u|^2_{H^2(\Omega_i)}.$$

The following regularity result holds [5]:

Theorem 2.1. *Assume that $f\in L^2(\Omega)$, $g_i\in H^{3/2}(\partial\Omega_i\cap\partial\Omega)$, for $i=1,2,3$. Then the problem* (2.1a)-(2.3) *has a unique solution $u\in H^1(\Omega)$ such that for some constant $C>0$,*

$$\|u\|_{\tilde{H}^2(\Omega)}\le C\left(\|f\|_{L^2(\Omega)}+\sum_{i=1}^{3}\|b_i\|_{H^{1/2}(\Gamma_i)}+\sum_{i=1}^{3}\|g_i\|_{H^{3/2}(\partial\Omega_i\cap\partial\Omega)}\right). \tag{2.5}$$

3 Immersed finite element method

Let $\mathcal{T}_h$ be an interface-independent triangulation of Ω. Since we do not require the mesh to be aligned with interfaces, $\mathcal{T}_h$ can be chosen as Cartesian mesh in actual computation. Let $\mathcal{N}_h$ be the set of all mesh points of $\mathcal{T}_h$. We denote by $\mathcal{N}_h^i=\mathcal{N}_h\cap\Omega$ and $\mathcal{N}_h^b=\mathcal{N}_h\cap\partial\Omega$ the collections of interior nodes and boundary nodes, respectively.

If the interfaces intersect the interior of an element, it is called an interface element; otherwise, it is called a non-interface element. The set of elements $\mathcal{T}_h$ is categorized into $\mathcal{T}_h^i$ and $\mathcal{T}_h^n$, representing the collections of interface elements and non-interface elements,

respectively. Particularly for this triple junction point problem, the set of interface elements $\mathcal{T}_h^i$ can be subdivided as follows

$$\begin{aligned}
\mathcal{T}_{h,1}^i &= \{T \in \mathcal{T}_h^i : T \text{ intersects only one interface among } \Gamma_1, \Gamma_2, \Gamma_3\},\\
\mathcal{T}_{h,2}^i &= \{T \in \mathcal{T}_h^i : T \text{ intersects two interfaces among } \Gamma_1, \Gamma_2, \Gamma_3\},\\
\mathcal{T}_{h,3}^i &= \{T \in \mathcal{T}_h^i : T \text{ intersects three interfaces among } \Gamma_1, \Gamma_2, \Gamma_3\}.
\end{aligned}$$

Then, we have

$$\mathcal{T}_h = \mathcal{T}_h^n \cup \mathcal{T}_{h,1}^i \cup \mathcal{T}_{h,2}^i \cup \mathcal{T}_{h,3}^i. \tag{3.1}$$

3.1 Local approximating functions

In this subsection, we construct the local approximating functions for each group of elements in (3.1). First, we note that if $T \in \mathcal{T}_h^n$, i.e., T is a non-interface element, then we use the standard P_1 finite element nodal basis functions. If $T \in \mathcal{T}_{h,1}^i$, then T only intersects with one interface. In this case, we follow the classical immersed finite element nodal basis construction as discussed in [23]. In the following, we focus on the remaining two cases.

3.1.1 The case $T \in \mathcal{T}_{h,2}^i$

In this case, the element T intersects with two interfaces, denoted by Γ_s and Γ_t. Their line approximation $\bar{\Gamma}_s = \overline{\Gamma_s^1 \Gamma_s^2}$ and $\bar{\Gamma}_t = \overline{\Gamma_t^1 \Gamma_t^2}$ are disjoint inside T. These two line segments subdivide the element T into three parts, denoted by T_a, T_b and T_c. See Fig. 2 for an illustration of the geometrical configuration of this case.

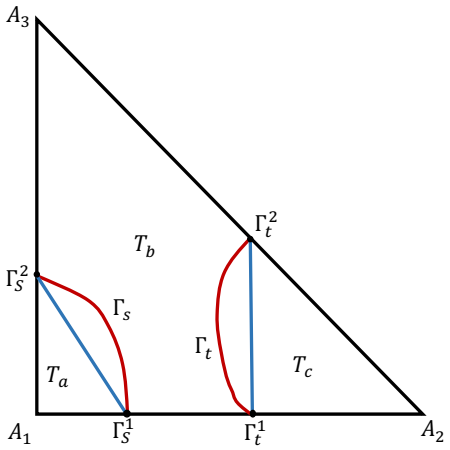

Figure 2: A typical element with two disjoint interfaces.

The local basis functions $\phi_{i,T}$, $i=1,2,3$, are formed as the following piecewise linear functions

$$\phi_{i,T}(\mathbf{x})=\begin{cases}\phi_{i,T}^{a}(\mathbf{x})=a_1x+b_1y+c_1, & \text{if } \mathbf{x}\in T_a,\\ \phi_{i,T}^{b}(\mathbf{x})=a_2x+b_2y+c_2, & \text{if } \mathbf{x}\in T_b,\\ \phi_{i,T}^{c}(\mathbf{x})=a_3x+b_3y+c_3, & \text{if } \mathbf{x}\in T_c.\end{cases} \tag{3.2}$$

For each basis function, there are nine coefficients to be determined. We impose the following conditions to determine these coefficients.

- three nodal value conditions

$$\phi_{i,T}(A_j)=\delta_{ij},\quad \forall j=1,2,3. \tag{3.3}$$

- four restrictions for the continuity of basis functions

$$\phi_{i,T}^{a}(\Gamma_s^l)=\phi_{i,T}^{b}(\Gamma_s^l),\quad \phi_{i,T}^{b}(\Gamma_t^l)=\phi_{i,T}^{c}(\Gamma_t^l),\quad \forall l=1,2. \tag{3.4}$$

- two restrictions for normal flux continuity

$$[\beta\nabla\phi_{i,T}\cdot\mathbf{n}]_{\Gamma_s}=0,\quad [\beta\nabla\phi_{i,T}\cdot\mathbf{n}]_{\Gamma_t}=0. \tag{3.5}$$

Direct calculation by verifying the determinant of the 9×9 matrix being nonzero yields the existence and uniqueness of the IFE basis functions. The local IFE space on T for homogeneous flux jump case is formed as $S_h(T)=span\{\phi_{1,T},\phi_{2,T},\phi_{3,T}\}$.

To handle the non-homogeneous flux jump conditions (2.3), we enrich the space $S_h(T)$ by adding two more piecewise linear basis functions $\phi_{T,J}^{s}$ and $\phi_{T,J}^{t}$ also in the form of (3.2) such that

$$\begin{aligned}&\phi_{T,J}^{s}(A_j)=0,\quad \forall j=1,2,3,\\ &[\phi_{T,J}^{s}(\bar{\Gamma}_s)]=0,\quad [\phi_{T,J}^{t}(\bar{\Gamma}_s)]=0,\\ &[\beta\nabla\phi_{T,J}^{s}\cdot\mathbf{n}]_{\Gamma_s}=1,\quad [\beta\nabla\phi_{T,J}^{s}\cdot\mathbf{n}]_{\Gamma_t}=0,\end{aligned}$$

and

$$\begin{aligned}&\phi_{T,J}^{t}(A_j)=0,\quad \forall j=1,2,3,\\ &[\phi_{T,J}^{t}(\bar{\Gamma}_s)]=0,\quad [\phi_{T,J}^{t}(\bar{\Gamma}_t)]=0,\\ &[\beta\nabla\phi_{T,J}^{t}\cdot\mathbf{n}]_{\Gamma_s}=0,\quad [\beta\nabla\phi_{T,J}^{t}\cdot\mathbf{n}]_{\Gamma_t}=1.\end{aligned}$$

We note that the matrix system for determine the homogeneous basis functions $\phi_{i,T}$ and the non-homogeneous basis functions $\phi_{T,J}^{s}$ and $\phi_{T,J}^{t}$ are exactly the same. Therefore, the existence and uniqueness of $\phi_{i,T}$ automatically imply the existence and uniqueness of $\phi_{T,J}^{t}$ and $\phi_{T,J}^{s}$. Define the local IFE flux jump space $S_h^J(T)=span\{\phi_{T,J}^{t},\phi_{T,J}^{s}\}$. Now the enriched

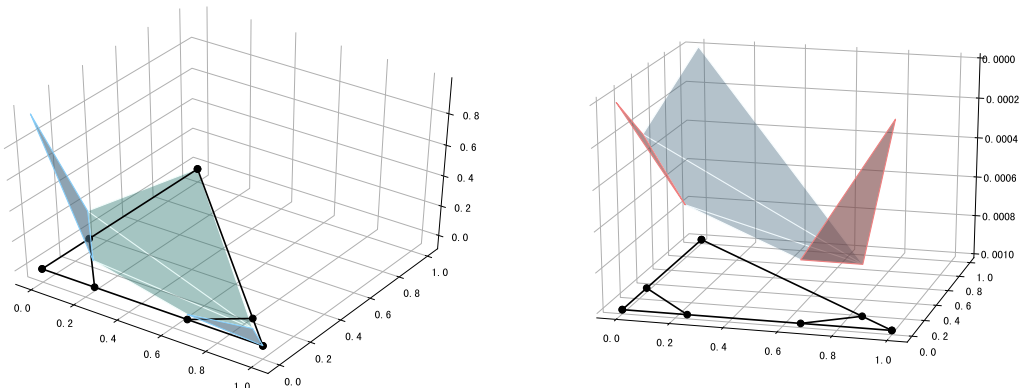

Figure 3: IFE basis function of 3.1.1 (left), flux jump function (right).

local IFE space on the element T is defined by $\tilde{S}_h(T)=S_h(T)\cup S_h^J(T)$. The Lagrange type interpolation $I_{h,T}:\tilde{H}^2(T)\to\tilde{S}_h(T)$ is defined as follows

$$I_{h,T}u(\mathbf{x})=\sum_{i=1}^{3}u(A_i)\phi_{i,T}(\mathbf{x})+q_T^s\phi_{T,J}^s(\mathbf{x})+q_T^t\phi_{T,J}^t(\mathbf{x}),\quad \mathbf{x}\in T. \tag{3.6}$$

Here, the arguments q_T^k, $k=s,t$ take the average of flux jump along the interface:

$$q_T^k=\frac{\int_{\Gamma_k\cap T}[\beta\nabla u\cdot\mathbf{n}]ds}{|\bar{\Gamma}_k|}, \tag{3.7}$$

where $|\bar{\Gamma}_k|$ is the length of $\bar{\Gamma}_k$. A typical IFE basis function and an IFE flux basis function are plotted in Fig. 3.

Remark 3.1. A special case for $T\in\mathcal{T}_{h,2}^i$ is that the intersection of two interfaces $\bar{\Gamma}_s$ and $\bar{\Gamma}_t$ is on the boundary of T, as depicted in Fig. 4. In this situation, the element T is still divided into three pieces, but two interface points Γ_s^1 and Γ_t^2 coincide. The construction of IFE basis functions follows exactly the same procedure.

3.1.2 The case $T\in\mathcal{T}_{h,3}^i$

In this case, the element T intersects with all three interfaces Γ_1, Γ_2 and Γ_3 at points Γ_1^0, Γ_2^0 and Γ_3^0, respectively. The line approximations of the interfaces are denoted by $\bar{\Gamma}_i=\overline{\Gamma_i^0P}$ where P is the triple junction point. There are two geometrical configurations in this case, which are illustrated in Fig. 5. The construction of the basis functions is quite similar for these two cases, so we only consider the one where the interfaces cut at three different edges of T.

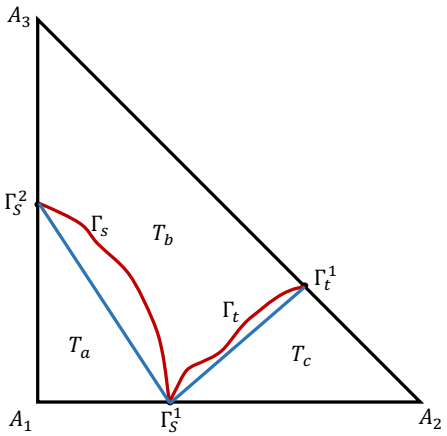

Figure 4: A special case of $T \in \mathcal{T}_{h,2}^i$.

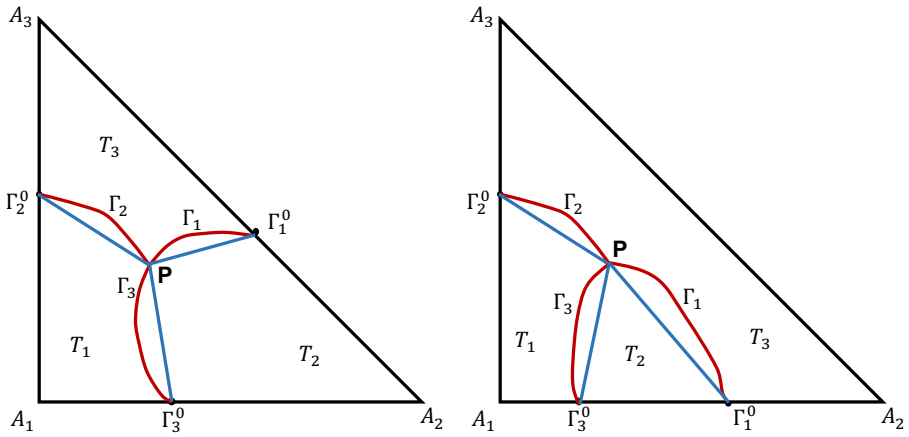

Figure 5: Two possible interface elements containing the triple junction point.

We construct the piecewise linear local basis functions $\phi_{i,T}$, $i=1,2,3$ in the following form

$$\phi_{i,T}(\mathbf{x}) = \begin{cases} \phi_{i,T}^1(\mathbf{x}) = a_1 x + b_1 y + c_1, & \text{if } \mathbf{x} \in T_1, \\ \phi_{i,T}^2(\mathbf{x}) = a_2 x + b_2 y + c_2, & \text{if } \mathbf{x} \in T_2, \\ \phi_{i,T}^3(\mathbf{x}) = a_3 x + b_3 y + c_3, & \text{if } \mathbf{x} \in T_3. \end{cases} \tag{3.8}$$

As before, we require the nodal-value and jump conditions as follows

- three nodal value conditions

$$\phi_{i,T}(A_j) = \delta_{ij}, \quad \forall i,j = 1,2,3. \tag{3.9}$$

- five continuity conditions of the basis functions

$$\phi^2_{i,T}(\Gamma^0_1)=\phi^3_{i,T}(\Gamma^0_1),\quad \phi^3_{i,T}(\Gamma^0_2)=\phi^1_{i,T}(\Gamma^0_2),\quad \phi^1_{i,T}(\Gamma^0_3)=\phi^2_{i,T}(\Gamma^0_3), \tag{3.10a}$$

$$\phi^1_{i,T}(P)=\phi^2_{i,T}(P),\quad \phi^2_{i,T}(P)=\phi^3_{i,T}(P). \tag{3.10b}$$

- three conditions of normal flux continuity

$$[\beta\nabla\phi_{i,T}\cdot\mathbf{n}]_{\bar{\Gamma}_1}=0,\quad [\beta\nabla\phi_{i,T}\cdot\mathbf{n}]_{\bar{\Gamma}_2}=0,\quad [\beta\nabla\phi_{i,T}\cdot\mathbf{n}]_{\bar{\Gamma}_3}=0. \tag{3.11}$$

We note that (3.9)-(3.11) provide eleven restrictions, which usually lead to an overdetermined linear system of nine unknowns in (3.8). As in [17], the least squares approximation is used to ensure the solvability of the system. After obtaining the basis functions, we can form the local IFE space $S_h(T)=span\{\phi_{1,T},\phi_{2,T},\phi_{3,T}\}$.

For the case with non-homogeneous jump, we enrich the local IFE space by adding three local functions $\phi^i_{T,J}$, $i=1,2,3$ such that

$$\phi^i_{T,J}(A_j)=0,\quad [\phi^i_{T,J}(\bar{\Gamma}_j)]=0,\quad [\beta\nabla\phi^i_{T,J}\cdot\mathbf{n}]_{\bar{\Gamma}_j}=\delta_{ij},\quad \forall j=1,2,3.$$

Define the local flux jump space by $S^J_h(T)=span\{\phi^1_{T,J},\phi^2_{T,J},\phi^3_{T,J}\}$. Then the enriched local IFE space on the element T is $\tilde{S}_h(T)=S_h(T)\cup S^J_h(T)$. The Lagrange type interpolation $I_{h,T}:\tilde{H}^2(T)\to\tilde{S}_h(T)$ is as follows

$$I_{h,T}u(X)=\sum_{i=1}^{3}u(A_i)\phi_{i,T}(X)+\sum_{k=1}^{3}q^k_T\phi^k_{T,J}(X), \tag{3.12}$$

where

$$q^k_T=\frac{\int_{\Gamma_k\cap T}[\beta\nabla u\cdot\mathbf{n}]ds}{|\bar{\Gamma}_k|}. \tag{3.13}$$

In Fig. 6 and Fig. 7, we plot IFE basis functions and the flux basis functions on triple junction interface elements of both geometrical configurations as in Fig. 5.

3.2 Global IFE space

Now we form the global IFE basis function by gluing together local basis functions that share the same node. Associated with each node $\mathbf{x}_i\in\mathcal{N}_h$ on the mesh, we define a global IFE basis function Φ_i such that the restriction $\Phi_i|_T$ is the local IFE basis functions we defined in previous subsection.

We define the global IFE space $S_h(\mathcal{T}_h)=span\{\Phi_i,i=1,2,\cdots,|\mathcal{N}_h|\}$ and the following two spaces taking into account of the boundary conditions

$$S^0_h(\mathcal{T}_h)=\{v\in S_h(\mathcal{T}_h):v(\mathbf{x})=0,\ \forall\mathbf{x}\in\mathcal{N}^b_h\},$$
$$S^g_h(\mathcal{T}_h)=\{v\in S_h(\mathcal{T}_h):v(\mathbf{x})=g(\mathbf{x}),\ \forall\mathbf{x}\in\mathcal{N}^b_h\}.$$

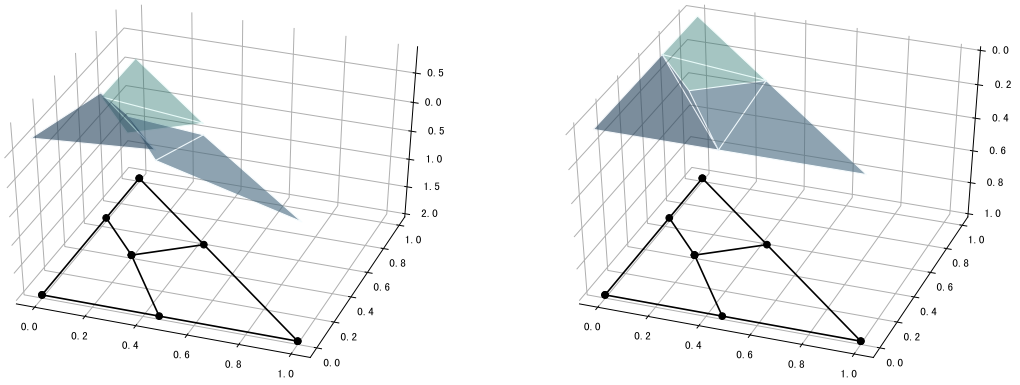

Figure 6: IFE basis function of 3.1.3 (left), flux jump function (right).

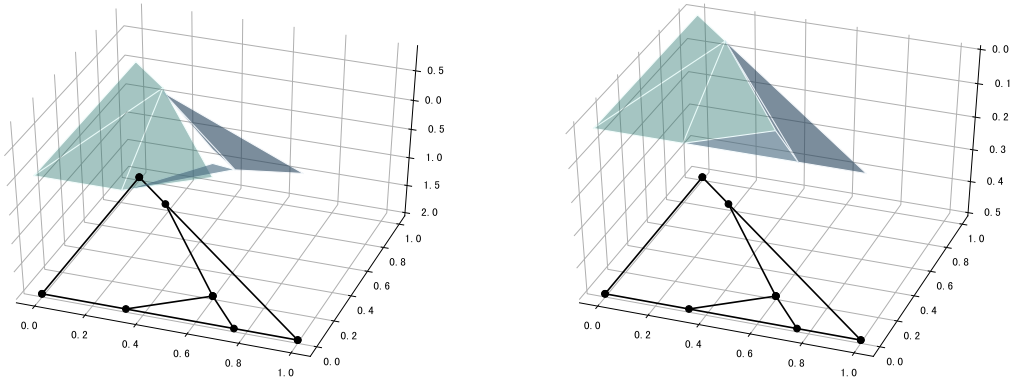

Figure 7: IFE basis function of 3.1.3 (left), flux jump function (right).

For non-homogeneous conditions, we define the global flux jump basis function as

$$\Phi^j_{T,J}(\mathbf{x}) = \begin{cases} \phi^j_{T,J}(\mathbf{x}), & \mathbf{x} \in T, \\ 0, & \mathbf{x} \notin T. \end{cases}$$

Here, the value j depends on the type of interface elements. The IFE flux jump space is defined as $S^J_h(\mathcal{T}_h) = span\{\Phi^j_{T,J},\ \forall T \in \mathcal{T}^i_h\}$. Then the enriched global IFE space can be written as $\tilde{S}_h(\mathcal{T}_h) = S_h(\mathcal{T}_h) \cup S^J_h(\mathcal{T}_h)$.

The IFE approximation is to find a function $\tilde{u}_h \in \tilde{S}_h(\mathcal{T}_h)$ in the following form

$$\tilde{u}_h = u_h + u^J_h = \sum_{i \in \mathcal{N}_h} u_i \Phi_i + \sum_{T \in \mathcal{T}^i_h} \sum_{j=1}^{3} q^j_T \Phi^j_{T,J}, \tag{3.14}$$

where the $u^J_h \in S^J_h(\mathcal{T}_h)$ is a function that we construct to approximate the non-homogeneous flux jump. The global interpolation operator $I_h : \tilde{H}^2(\Omega) \to \tilde{S}_h(\mathcal{T}_h)$ is defined in the standard

manner as

$$I_h(u)|_T = I_{h,T}(u), \quad \forall T \in \mathcal{T}_h.$$

Finally, the IFE method for solving the interface problem (2.1a)-(2.3) is to find $u_h \in S_h^g(\mathcal{T}_h)$ such that

$$\sum_{T\in\mathcal{T}_h}\int_T \beta\nabla_h u_h\cdot\nabla_h v d\mathbf{x} = \int_\Omega f v d\mathbf{x} - \sum_{k=1}^{3}\int_{\Gamma_k} b_k v ds - \int_\Omega \beta\nabla_h u_h^I\cdot\nabla_h v d\mathbf{x}, \quad \forall v \in S_h^0(\mathcal{T}_h), \quad (3.15)$$

where ∇_h denotes the broken gradient operator that operates on each piece of the element.

Remark 3.2. The bilinear form on the left hand side of (3.15) is symmetric. The resulting stiffness matrix of numerical scheme (3.15) is symmetric positive definite.

Remark 3.3. For multi-domain problems with more than three interfaces, the idea of construction of the IFE basis functions can be extended naturally. Least squares approximation will be used for multiple intersecting interfaces.

4 Numerical experiments

In this section, we present some numerical examples to test the performance of the new IFE method.

Example 4.1. In this example, we consider a domain separated by three straight line interfaces. Let $\Omega = (-1,1)^2$. The interfaces are defined through the level set functions φ_i as follows

$$\begin{aligned}\varphi_1(x,y) &= x+0.1y-0.055,\\ \varphi_2(x,y) &= x+0.2y-0.06,\\ \varphi_3(x,y) &= 0.03x+y-0.0515.\end{aligned}$$

The coefficient functions $(\beta_1,\beta_2,\beta_3) = (10,1,100)$. The exact solution of this problem is

$$\begin{aligned}u_1(x,y) &= \frac{1}{\beta_1}\sin(y+0.03x-0.0515)(x+0.2y-0.06),\\ u_2(x,y) &= \frac{1}{\beta_2}\sin(y+0.03x-0.0515)(x+0.1y-0.055),\\ u_3(x,y) &= \frac{1}{\beta_3}\sin(0.1y+x-0.055)(x+0.2y-0.06).\end{aligned}$$

We use a family of uniformly refined Cartesian triangular meshes that consists of $2\times n_x\times n_y$ triangles. The errors of interpolation using new IFE space are reported in Table 1. We can observe that both L^2 norm and H^1 norms seem to converge in optimal rate for linear approximation. The errors of Galerkin IFE solutions are reported in Table 2. Fig. 8 displays the numerical solution on the 64×64 mesh.

Table 1: Interpolation Error of Example 4.1 with $(\beta_1,\beta_2,\beta_3)=(10,1,100)$.

$n_x\times n_y$	$\|\|I_hu-u\|\|_{L^2}$	order	$\|I_hu-u\|_{H^1}$	order
16×16	1.5087×10^{-3}		6.0104×10^{-2}	
32×32	3.7538×10^{-4}	2.01	3.0320×10^{-2}	0.99
64×64	9.2808×10^{-5}	2.02	1.5168×10^{-2}	1.00
128×128	2.3133×10^{-5}	2.00	7.5879×10^{-3}	1.00

Table 2: Galerkin IFE Solution Error of Example 4.1 with $(\beta_1,\beta_2,\beta_3)=(10,1,100)$.

$n_x\times n_y$	$\|\|u_h-u\|\|_{L^2}$	order	$\|u_h-u\|_{H^1}$	order
16×16	1.5436×10^{-3}		6.3291×10^{-2}	
32×32	3.9297×10^{-4}	1.97	3.1879×10^{-2}	0.99
64×64	8.2307×10^{-5}	2.26	1.5717×10^{-2}	1.02
128×128	2.3532×10^{-5}	1.81	7.8775×10^{-3}	1.00

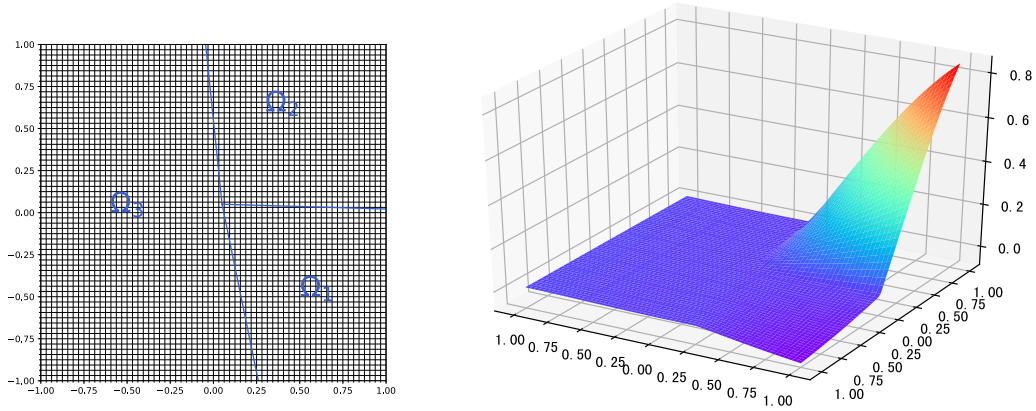

Figure 8: The interface geometry and the numerical solution for Example 4.1.

Example 4.2. The second example is to test the capability of our numerical method for the case when the triple junction point lies on the grid point. The domain $\Omega=(-1,1)^2$ and the level set functions φ_i are defined as follows

$$\begin{aligned}\varphi_1(x,y)&=x+0.1y,\\ \varphi_2(x,y)&=x+0.2y,\\ \varphi_3(x,y)&=0.03x+y.\end{aligned}$$

This is a translation of the exact solution in Example 4.1. The exact solution of this problem is

$$u_1(x,y)=\frac{1}{\beta_1}\sin(y+0.03x)(x+0.2y),$$

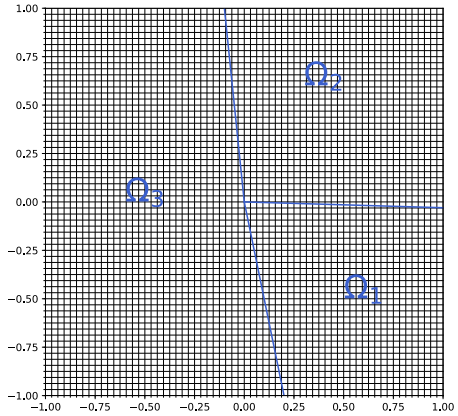

Figure 9: The interface geometry for Example 4.2.

Table 3: Interpolation Error of Example 4.2 with $(\beta_1,\beta_2,\beta_3)=(10,1,100)$.

$n_x\times n_y$	$\|\|I_hu-u\|\|_{L^2}$	order	$\|I_hu-u\|_{H^1}$	order
10×10	4.0917×10^{-3}		1.0035×10^{-1}	
20×20	1.0176×10^{-3}	2.01	5.0309×10^{-2}	1.00
40×40	2.5319×10^{-4}	2.01	2.5182×10^{-2}	1.00
80×80	6.2934×10^{-5}	2.01	1.2595×10^{-2}	1.00
160×160	1.5697×10^{-5}	2.00	6.2998×10^{-3}	1.00

Table 4: Galerkin IFE Solution Error of Example 4.2 with $(\beta_1,\beta_2,\beta_3)=(10,1,100)$.

$n_x\times n_y$	$\|\|u_h-u\|\|_{L^2}$	order	$\|u_h-u\|_{H^1}$	order
10×10	3.8956×10^{-3}		1.1554×10^{-1}	
20×20	1.0235×10^{-3}	1.93	5.3793×10^{-2}	1.10
40×40	2.3212×10^{-4}	2.14	2.6246×10^{-2}	1.04
80×80	5.9050×10^{-5}	1.97	1.3063×10^{-2}	1.01
160×160	1.6664×10^{-5}	1.82	6.5707×10^{-3}	0.99

$$u_2(x,y)=\frac{1}{\beta_2}\sin(y+0.03x)(x+0.1y),$$
$$u_3(x,y)=\frac{1}{\beta_3}\sin(0.1y+x)(x+0.2y).$$

We use a different set of triangular mesh starting from a 10×10 partition. In this way, the triple junction point will coincide with a mesh point. See Fig. 9 for the geometrical setting of this example. A small perturbation of 0.001 times the mesh size is used to ensure the local system is solvable. The errors of interpolation and Galerkin IFE solution are reported in Table 3 and Table 4, respectively. The numerical result shows that the method is robust in terms of the location of the triple junction point. The error decay rate

is similar as in previous example.

Example 4.3. In this example, we test our numerical scheme for curved interfaces. In particular, the interfaces consist of a circle and a straight line. The interfaces are defined by the level set functions

$$\begin{aligned}\varphi_1(x,y)&=4y-3x,\\ \varphi_2(x,y)&=-x^2-y^2+0.25,\\ \varphi_3(x,y)&=x^2+y^2-0.25.\end{aligned}$$

The coefficient function is chosen as $(\beta_1,\beta_2,\beta_3)=(10,1,100)$. The exact solution is as follows

$$\begin{aligned}u_1(x,y)&=\frac{1}{\beta_1}((x^2+y^2)^{1.5}-0.125),\\ u_2(x,y)&=\frac{1}{\beta_2}(x^2+y^2-0.25)\sin(3x-4y),\\ u_3(x,y)&=\frac{1}{\beta_3}(3x-4y)\ln(x^2+y^2+0.75).\end{aligned}$$

To demonstrate the robustness of the numerical scheme with respect to the interface location, we use two different families of meshes. In Table 5 and Table 6, we report the interpolation and Galerkin solution on a sequence of meshes starting from a 16×16 mesh. In Table 7 and Table 8 we report the numerical results on a sequence of mesh starting from a 10×10 mesh. Moreover, Fig. 10 shows the numerical solution on the 64×64 mesh.

Table 5: Interpolation Error of Example 4.3 with $(\beta_1,\beta_2,\beta_3)=(10,1,100)$.

$n_x\times n_y$	$\|\|I_hu-u\|\|_{L^2}$	order	$\|I_hu-u\|_{H^1}$	order
16×16	3.7273×10^{-2}		1.0526×10^{0}	
32×32	9.4653×10^{-3}	1.98	5.3219×10^{-1}	0.98
64×64	2.3750×10^{-3}	1.99	2.6690×10^{-1}	1.00
128×128	5.9428×10^{-4}	2.00	1.3357×10^{-1}	1.00

Table 6: Galerkin IFE Solution Error of Example 4.3 with $(\beta_1,\beta_2,\beta_3)=(10,1,100)$.

$n_x\times n_y$	$\|\|u_h-u\|\|_{L^2}$	order	$\|u_h-u\|_{H^1}$	order
16×16	1.3296×10^{-2}		1.0652×10^{0}	
32×32	2.7358×10^{-3}	2.28	5.3537×10^{-1}	0.99
64×64	6.0644×10^{-4}	2.17	2.6790×10^{-1}	1.00
128×128	1.5761×10^{-4}	1.94	1.3403×10^{-1}	1.00

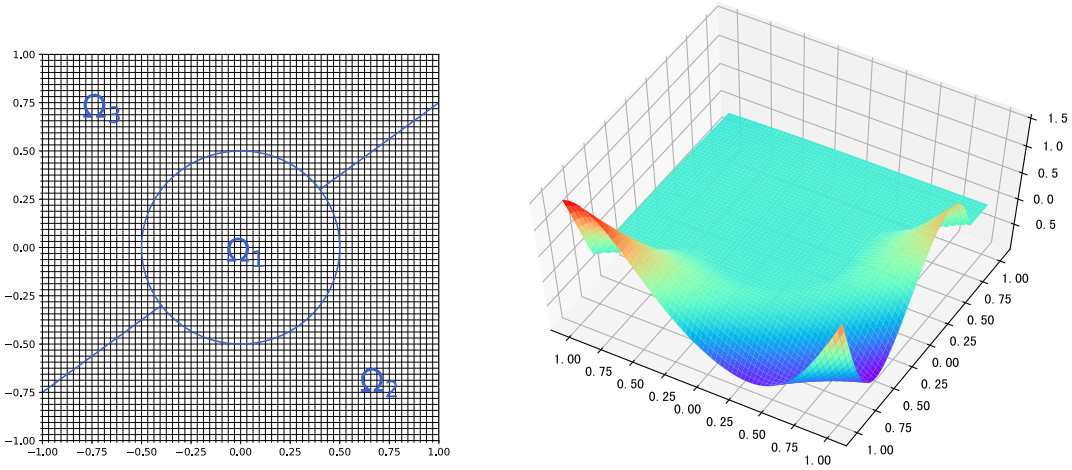

Figure 10: The interface geometry and numerical solution for Example 4.3.

Table 7: Interpolation Error of Example 4.3 with $(\beta_1,\beta_2,\beta_3)=(10,1,100)$ on different meshes.

$n_x\times n_y$	$\|\|I_hu-u\|\|_{L^2}$	order	$\|I_hu-u\|_{H^1}$	order
10×10	9.2212×10^{-2}		1.6465×10^{0}	
20×20	2.4053×10^{-2}	1.94	8.4657×10^{-1}	0.96
40×40	6.0691×10^{-3}	1.99	4.2637×10^{-1}	0.99
80×80	1.5207×10^{-3}	2.00	2.1361×10^{-1}	1.00
160×160	3.8037×10^{-4}	2.00	1.0687×10^{-1}	1.00

Table 8: Galerkin IFE Solution Error of Example 4.3 with $(\beta_1,\beta_2,\beta_3)=(10,1,100)$ on different meshes.

$n_x\times n_y$	$\|\|u_h-u\|\|_{L^2}$	order	$\|u_h-u\|_{H^1}$	order
10×10	3.4518×10^{-2}		1.6876×10^{0}	
20×20	8.2927×10^{-3}	2.06	8.5755×10^{-1}	0.98
40×40	1.6023×10^{-3}	2.37	4.2850×10^{-1}	1.00
80×80	3.6388×10^{-4}	2.14	2.1434×10^{-1}	1.00
160×160	9.2892×10^{-5}	1.97	1.0727×10^{-1}	1.00

5 Conclusions

In this paper, we develop an immersed finite element method to solve multi-domain interface problem with triple junction points. We categorize elements according to their geometric configurations. In the element that contains the triple junction points, we use least squares fitting to uniquely determine the IFE basis functions. The numerical experiments show the interpolation could achieve second order accuracy measured by L^2 norm and first order in H^1 norm. The Galerkin method using this IFE functions is symmetric positive definite. They can provide reasonably accurate solutions to the multi-domain

interface problems.

Acknowledgements

S. Hou's research is supported by Dr. Walter Koss Endowed Professorship. This professorship is made available through the State of Louisiana Board of Regents Support Funds. X. Zhang's research is partially supported by National Science Foundation Grant DMS-1720425.

References

[1] S. ADJERID, N. CHAABANE AND T. LIN, *An immersed discontinuous finite element method for stokes interface problems,* Comput. Methods Appl. Mech. Eng., 293 (2015), pp. 170–190.
[2] S. ADJERID, R. GUO AND T. LIN, *High degree immersed finite element spaces by a least squares method,* Int. J. Numer. Anal. Model., 14(4-5) (2017), pp. 604–626.
[3] S. ADJERID AND T. LIN, *Higher-order immersed discontinuous Galerkin methods,* Int. J. Inf. Syst. Sci., 3(4) (2007), pp. 555–568.
[4] I. BABUSKA AND U. BANERJEE, *Stable generalized finite element method (SGFEM),* Comput. Methods Appl. Mech. Eng., 201/204 (2012), pp. 91–111.
[5] J. H. BRAMBLE AND J. T. KING, *A finite element method for interface problems in domains with smooth boundaries and interfaces,* Adv. Comput. Math., 6(2) (1996), pp. 109–138.
[6] W. CAO, X. ZHANG AND Z. ZHANG, *Superconvergence of immersed finite element methods for interface problems,* Adv. Comput. Math., 43(4) (2017), pp. 795–821.
[7] W. CAO, X. ZHANG, Z. ZHANG AND Q. ZOU, *Superconvergence of immersed finite volume methods for one-dimensional interface problems,* J. Sci. Comput., 73(2-3) (2017), pp. 543–565.
[8] Z. CHEN AND J. ZOU, *Finite element methods and their convergence for elliptic and parabolic interface problems*, Numer. Math., 79(2) (2017), pp. 175–202.
[9] A. L. FOGELSON AND J. P. KEENER, *The extended/generalized finite element method: an overview of the method and its applications*, Int. J. Numer. Methods Eng., 84(3) (2010), pp. 253–304.
[10] H. GUO AND X. YANG, *Gradient recovery for elliptic interface problem: II. Immersed finite element methods,* J. Comput. Phys., 338 (2017), pp. 606–619.
[11] Y. GONG, B. LI AND Z. LI, *Immersed-interface finite-element methods for elliptic interface problems with nonhomogeneous jump conditions,* SIAM J. Numer. Anal., 46(1) (2007/08), pp. 472–495,
[12] A. HANSBO AND P. HANSBO, *An unfitted finite element method, based on Nitsche's method, for elliptic interface problems,* Comput. Methods Appl. Mech. Eng., 191(47-48) (2002), pp. 5537–5552.
[13] X. HE, T. LIN AND Y. LIN, *Approximation capability of a bilinear immersed finite element space,* Numer. Methods Partial Differential Equations, 24(5) (2008), pp. 1265–1300.
[14] X. HE, T. LIN AND Y. LIN, *Immersed finite element methods for elliptic interface problems with non-homogeneous jump conditions,* Int. J. Numer. Anal. Model., 8(2) (2011), pp. 284–301.
[15] X. HE, T. LIN, Y. LIN AND X. ZHANG, *Immersed finite element methods for parabolic equations with moving interface,* Numer. Methods Partial Differential Equations, 29(2) (2013), pp. 619–646.

[16] D. W. HEWETT, *The embedded curved boundary method for orthogonal simulation meshes,* J. Comput. Phys., 138 (1997), pp. 585–616.
[17] S. HOU, L. WANG AND W. WANG, *A numerical method for solving the elliptic interface problems with multi-domains and triple junction points,* J. Comput. Math., 30(5) (2012), pp. 504–516.
[18] S. HOU, W. WANG AND L. WANG, *Numerical method for solving matrix coefficient elliptic equation with sharp-edged interfaces,* J. Comput. Phys., 229(19) (2010), pp. 7162–7179.
[19] D. M. INGRAM, D. M. CAUSON AND C. G. MINGHAM, *Developments in cartesian cut cell methods,* Math. Comput. Simulation, 61(3-6) (2003), pp. 561–572.
[20] R. J. LEVEQUE AND Z. LI, *The immersed interface method for elliptic equations with discontinuous coefficients and singular sources,* SIAM J. Numer. Anal., 31(4) (1994), pp. 1019–1044.
[21] Z. LI, *The immersed interface method using a finite element formulation,* Appl. Numer. Math., 27(3) (1998), pp. 253–267.
[22] Z. LI, T. LIN AND X. WU, *New Cartesian grid methods for interface problems using the finite element formulation*, Numer. Math., 96(1) (2003), pp. 61–98.
[23] T. LIN, Y. LIN AND X. ZHANG, *Partially penalized immersed finite element methods for elliptic interface problems,* SIAM J. Numer. Anal., 53(2) (2015), pp. 1121–1144.
[24] T. LIN, D. SHEEN AND X. ZHANG, *A locking-free immersed finite element method for planar elasticity interface problems,* J. Comput. Phys., 247 (2013), pp. 228–247.
[25] C. S. PESKIN, *Numerical analysis of blood flow in the heart,* J. Comput. Phys., 25(3) (1977), pp. 220–252.
[26] L. WANG, S. HOU AND L. SHI, *A numerical method for solving three-dimensional elliptic interface problems with triple junction points,* Adv. Comput. Math., 44(1) (2018), pp. 175–193.
[27] L. WANG, S. HOU, L. SHI AND J. SOLOW, *A numerical method for solving elasticity equations with interface involving multi-domains and triple junction points,* Appl. Math. Comput., 251 (2015), pp. 615–625.
[28] K. L. XIA, M. ZHAN AND G. W. WEI, *MIB method for elliptic equations with multi-material interfaces,* J. Comput. Phys., 230(12) (2011), pp. 4588–4615.
[29] W. YING AND C. S. HENRIQUEZ, *A kernel-free boundary integral method for elliptic boundary value problems,* J. Comput. Phys., 227(2) (2007), pp. 1046–1074.
[30] S. YU, Y. ZHOU AND G. W. WEI, *Matched interface and boundary (MIB) method for elliptic problems with sharp-edged interfaces,* J. Comput. Phys., 224(2) (2007), pp. 729–756.